American Mineralogist, Volume 91, pages 809–815, 2006

The effect of Ca substitution on the elastic and structural behavior of orthoenstatite

FABRIZIO NESTOLA,* G. DIEGO GATTA,† AND TIZIANA BOFFA BALLARAN

Bayerisches Geoinstitut, Universitaet Bayreuth, Universitaetstrasse 30, D-95447, Bayreuth, Germany

ABSTRACT

A single crystal of orthopyroxene with composition $Ca_{0.07}Mg_{1.93}Si_2O_6$ (space group *Pbca*) has been investigated at high pressure and room temperature by in-situ X-ray diffraction using a diamond anvil cell. The unit-cell parameters have been determined at ten different pressures up to 10.16(5) GPa. In the pressure range investigated no evidences of phase transitions have been found. The pressure-volume data have been fitted with a third-order Birch-Murnaghan equation of state resulting in the following parameters: V_0 = 838.26(8) Å^3, K_{T0} = 110(1) GPa, K' = 6.6(4). The Ca substitution in the pure orthoenstatite $Mg_2Si_2O_6$ structure causes a slight increase in K_{T0} and a decrease in K'. The compressibility of *a*, *b*, and *c* unit-cell parameters is strongly anisotropic with a compressibility scheme $\beta_b >> \beta_c >> \beta_a$. The structure evolution as a function of pressure has been determined at five different pressures up to 6.25(5) GPa. The M2 polyhedron undergoes the largest volume variation (~7.7%), whereas the volume variation of M1 is ~6.1%. The TA and TB tetrahedral volumes decrease by about 3% and 1.2%, respectively, without a discontinuity in the pressure range investigated.

Keywords: Orthopyroxene, high-pressure, compressibility, equation of state

INTRODUCTION

Orthopyroxenes, and in particular the pure end-member orthoenstatite (Oen, $Mg_2Si_2O_6$, space group *Pbca*), are among the most studied silicates in Earth Sciences. Such interest is due to their abundance into the Earth's lower crust and upper mantle. They are also among the most abundant phases present in volcanic rocks and in meteorites as mesosiderites (Ganguly et al. 1994), lodranites, acapulocites, diogenites, howardites, ureilites, and shergottites (Molin et al. 1994; Zema et al. 1996, 1997; Domeneghetti et al. 2000; Goodrich et al. 2001; Goodrich 2003). Knowledge of their thermodynamic properties allows us to determine accurately the temperature and pressure conditions at which these minerals are formed and to constrain the formation conditions of important rock assemblages in the Earth's deep interior. The crystal chemistry of more than 200 natural orthopyroxenes has been determined by Domeneghetti et al. (1995a) who obtained linear equations that allow the prediction of cell parameters and interatomic distances for any orthopyroxene, starting from its chemical formula. Several studies of the crystal chemistry and elastic properties at room conditions have been performed on pure orthoenstatite (Morimoto and Koto 1969; Hawthorne and Ito 1977; Weidner et al. 1978; Ohashi 1984; Yang and Ghose 1995a; Duffy and Vaughan 1998; Jackson et al. 1999) and along the join $Mg_2Si_2O_6$–$Fe_2Si_2O_6$ (orthoferrosilite), since Fe^{2+}/Mg is the major cation substitution occurring in orthopyroxenes (Bass and Weidner 1984; Domeneghetti and Steffen 1992; Skogby et al. 1992; Yang and Ghose 1995b). Numerous investigations along this join have also been carried out both at high-pressure (Frisillo and Barsch 1972; Ito et al. 1977; Weidner et al. 1978; Ralph and Ghose 1980; Webb and Jackson 1993; Angel and Hugh-Jones 1994; Hugh-Jones et al. 1997; Woodland 1998; Chai et al. 1997; Flesch et al. 1998; Jackson et al. 1999; Angel and Jackson 2002; Lin 2003; Kung et al. 2004) and at high temperature (Chopelas and Boehler 1992; Yang and Ghose 1994; Zhao et al. 1995; Hugh-Jones 1997; Chopelas 2000; Jackson et al. 2001, 2004). The elasticity and equation of state (EoS) of orthopyroxenes have been the subject of controversy for the last few decades. In a recent study, Angel and Jackson (2002) addressed the discrepancies among EoS parameters previously reported for orthoenstatite. They re-analyzed published measurements of compression and elasticity of Oen, and showed that the revised room pressure bulk modulus (K_{T0}) and its pressure derivative (K') are indeed consistent with one another as well as with new single-crystal compression data presented in the same paper. The best estimates of K_{T0} = 105.8(5) GPa and of K' = 8.5(3), using a third-order Birch-Murnhagan (BM3; Birch 1947) EoS, confirm that orthoenstatite (and very likely also orthoferrosilite; Hugh-Jones et al. 1997) has an "anomalously" high value of K' at room temperature. It appears, therefore, that Fe^{2+} substitution has little effect on the compressibility of orthoenstatite (Hugh-Jones et al. 1997). However, some investigations indicate that the Fe^{2+} substitution has an effect on the elasticity of orthoenstatite (Bass and Weidner 1984; Duffy and Vaughan 1988; Jackson et al. 1999), although the effect seems to be more pronounced for shear elasticity and there is some debate concerning its effect on the bulk modulus (Jackson et al. 1999).

Natural orthopyroxenes, however, seem to behave differently, probably due to the presence of other cations, like Al or Ca, which may play a crucial role in determining the elastic and compressional behavior of these minerals. A few studies have

* Present address: Dipartimento di Mineralogia e Petrologia, Università degli Studi di Padova, Corso Garibaldi 37, I-35137, Padova, Italy. E-mail: fabrizio.nestola@unipd.it

† Present address: Dipartimento di Scienze della Terra, Università di Milano, Via Botticelli 23, I-20133, Milano, Italy.

0003-004X/06/0506–809$05.00/DOI: 10.2138/am.2006.1982

been performed at room conditions on natural Ca-orthopyroxenes (Chatillon-Colinet et al. 1983; Domeneghetti et al. 1995b; Zema et al. 1999; Stimpfl et al. 1999). Zema et al. (2003) showed that Ca occupies the M2 sites causing an enlargement of this polyhedron but it does not affect the kinetics of the Fe-Mg non-convergent ordering process. Single-crystal structure determinations up to 6 GPa of a natural orthopyroxene (Hugh-Jones et al. 1997) show that chemical substitution of Al and Ca into the structure of orthopyroxene inhibits the initial rapid compression of M2-O3 bonds and the significant tetrahedral compression above 4 GPa observed in synthetic $(Mg,Fe)SiO_3$ samples. In natural samples, however, it is difficult to discriminate among the effects of the different cations, and only the overall effect of minor cations can be described.

The first study focusing on the effect of Ca alone on the orthoenstatite structure was performed along the synthetic join diopside ($CaMgSi_2O_6$)–enstatite (Nestola and Tribaudino 2003). That study demonstrated that substitution of Ca in the *Pbca* structure of orthoenstatite induces local distortions of the tetrahedral chains, which destabilize the structure. This suggests that the orthoenstatite structure cannot contain more than 9–10% of Ca apfu, as observed in natural samples (Domeneghetti et al. 1995a). For Ca contents of ~15%, the stable phase appears to be that of pigeonite with $P2_1/c$ symmetry at room conditions (Tribaudino and Nestola 2002).

In this study, high-pressure experiments have been performed on one of the samples synthesized by Nestola and Tribaudino (2003), an iron-free orthopyroxene with composition $Ca_{0.07}Mg_{1.93}Si_2O_6$. The purpose is to determine if Ca alone may be responsible for the difference between the high-pressure behavior of natural orthopyroxenes and orthoenstatite (Hugh-Jones et al. 1997).

Experimental methods

The orthopyroxene sample used in this study has been accurately characterized by means of transmission electron microscopy (TEM), X-ray diffraction, and SEM-EDS (Nestola and Tribaudino 2003). Two single crystals of different sizes were selected from this sample for high-pressure unit-cell determination ($80 \times 50 \times 30$ μm^3) and intensity-data collection ($250 \times 155 \times 55$ μm^3). The authors reported the presence of 0*kl* reflections violating the *b* glide, which they related to the presence of clinopyroxene lamellae oriented parallel to (100); however, only a few of these reflections (those with $l = 2n$) appear to have intensity $\geq 2\sigma$.

High-pressure single-crystal diffraction experiments were performed with BGI design diamond-anvil cells (Allan et al. 1996), using steel gaskets pre-indented to thicknesses of 50 and 120 μm, and with hole diameters of 250 and 350 μm, for the smaller and larger crystals, respectively. Ruby chips were used as internal pressure standards and a 16:3:1 mixture of methanol:ethanol:water was used as hydrostatic pressure medium. Unit-cell parameter measurements were performed on a Huber single-crystal diffractometer by centering a list of 20 reflections, which are related exclusively to the orthopyroxene structure (the 0*kl*, $l = 2n$ reflections were excluded from the list). Full details of the instrument and the peak-centering algorithm are provided by Angel et al. (2000). The values of symmetry-constrained unit-cell parameters obtained by vector-least-squares (Ralph and Finger 1982) are reported in Table 1.

Intensity data were collected at different pressures up to 6.25 GPa both during compression and decompression using a Kappa geometry Xcalibur diffractometer with graphite monochromated Mo$K\alpha$ radiation. Equivalent sets of reflections *hkl*, $h\bar{k}l$, and $hk\bar{l}$ were measured in the $5 \leq 2\theta \leq 60°$ range using the ω-scan mode with a continuous-integrative step scan (0.05°/s, 60 scan steps, scan width 1.2°) under ambient conditions. The sample-detector distance was 135 mm. The program WinIntegrStp (version 3.3, Angel 2003) was used to integrate the step-scan data applying the Lorentz-polarization correction. The intensity data were corrected for absorption using the program ABSORB V6.0 (Angel 2004). Weighted structural refinements were done using the SHELX-97 package (Sheldrick 1997); atomic scattering factors were taken from the *International Tables for X-Ray Crystallography* (Wilson 1995). The refinements were performed in space group *Pbca*, using the room-temperature coordinates of Nestola and Tribaudino (2003) as starting parameters in the refinement. Anisotropic displacement parameters were obtained for all atoms only in the structure refinement based on room pressure data, which was obtained from the crystal in air. In the structure refinements at high-pressure, anisotropic displacement parameters were determined only for the M2 and M1 sites, with occupancy of Mg and Ca of the M2 site constrained to the values obtained from the chemical analysis (0.93 and 0.07 apfu, respectively; Nestola and Tribaudino 2003). Refinement details, atomic coordinates, displacement parameters, and interatomic distances and angles are reported in Tables 2, 3, and 4.

Results

Elastic behavior

The unit-cell parameters measured at ten different pressures up to 10.16(5) GPa are reported in Figure 1. The data points at 9.40, 7.49, and 2.80 GPa were measured while decompressing and they do not show any deviation from the trends obtained during compression. No evidence of a phase transition was found. The pressure-volume data were fitted by a BM3 EoS (Birch 1947) refining simultaneously unit-cell volume, V_0, bulk modulus, K_{T0}, and its first pressure derivative, K'. The refinement was performed using the program EOSFIT 5.2 (Angel 2001), which yielded the following EoS parameters: $V_0 = 838.26(8)$ Å^3, $K_{T0} = 110(1)$ GPa, $K' = 6.6(4)$. The normalized strain vs. finite strain plot (F_E-f_E plot; Angel 2000) confirms that the *P*-*V* data are adequately described by a BM3 fit (Fig. 2).

The compressibility of *a*, *b*, and *c* unit-cell parameters is strongly anisotropic (Fig. 1). Linearized F_E-f_E plots, obtained by substituting the cube of the unit-cell lattice parameters for the volume in the normalized strain and finite strain equations

Table 1. Variation of unit-cell parameters with pressure for the Ca-orthoenstatite sample

P (GPa)	*a* (Å)	*b* (Å)	*c* (Å)	*V* (Å^3)
0.00010(1)	18.2718(4)	8.8323(2)	5.1941(4)	838.24(8)
1.51(5)	18.2150(6)	8.7859(3)	5.1719(6)	827.60(8)
2.80(5)*	18.1659(6)	8.7459(7)	5.1545(1)	818.93(14)
2.81(5)	18.1658(4)	8.7460(3)	5.1539(6)	818.84(8)
3.78(5)	18.1342(6)	8.7176(4)	5.1400(7)	812.57(8)
5.35(5)	18.0780(5)	8.6750(3)	5.1221(6)	803.29(8)
7.28(5)	18.0170(6)	8.6280(6)	5.1005(11)	792.87(11)
7.49(5)*	18.0159(10)	8.6249(1)	5.0974(20)	792.07(28)
9.40(5)*	17.9563(5)	8.5796(5)	5.0801(8)	782.62(12)
10.16(5)	17.9416(5)	8.5642(7)	5.0740(7)	779.64(7)

Note: The uncertainties in pressure is from Mao et al. (1986).
* Data measured under decompression.

Table 2. Structure refinement results for the Ca-orthoenstatite sample

	0.0001 GPa	1.76 GPa	3.36 GPa	3.94 GPa	6.25 GPa
a (Å)	18.2588(5)	18.201(1)	18.093(2)	18.108(2)	18.022(1)
b (Å)	8.8229(5)	8.768(1)	8.750(1)	8.7215(9)	8.6578(6)
c (Å)	5.1899(5)	5.154(1)	5.127(2)	5.120(1)	5.085(1)
V (Å^3)	836.07(9)	822.6(2)	811.7(4)	808.6(2)	793.4(2)
S.G.	*Pbca*	*Pbca*	*Pbca*	*Pbca*	*Pbca*
Uniq. refl.	1050	312	457	345	322
R_{int}(%)	2.39	5.17	7.16	5.49	5.72
$R4\sigma$(%)	2.60	6.36	6.59	5.18	6.28
R_{all}(%)	2.71	8.80	7.85	7.08	7.42
GooF	1.1	1.1	1.2	1.0	0.9
NP	94	52	52	52	52

Notes: The data at 1.76 and 3.94 GPa were measured during decompression. The refinement at 0 GPa is for the crystal in air.

TABLE 3. Atomic fractional coordinates and thermal parameters (Å²)

Pressure		0.0001 GPa	1.76 GPa	3.36 GPa	3.94 GPa	6.25 GPa
M2	*x*	0.37693(3)	0.3768(3)	0.3772(2)	0.3772(2)	0.3779(3)
	y	0.48481(7)	0.4829(4)	0.4823(3)	0.4828(3)	0.4811(5)
	z	0.36233(12)	0.3597(11)	0.3548(9)	0.3549(7)	0.3530(12)
	U_{11}	0.0098(3)	0.012(3)	0.008(2)	0.004(2)	0.009(3)
	U_{22}	0.0122(3)	0.013(2)	0.013(1)	0.013(1)	0.012(2)
	U_{33}	0.0085(3)	0.016(4)	0.009(4)	0.016(3)	0.014(4)
	U_{12}	−0.0026(2)	−0.003(2)	−0.003(1)	0.004(2)	0.001(2)
	U_{13}	−0.0016(2)	−0.004(2)	0.001(1)	−0.002(1)	0.003(2)
	U_{23}	−0.0016(2)	−0.005(2)	−0.006(2)	−0.003(2)	−0.005(3)
	U_{eq}/U_{iso}	0.0102(2)	0.014(1)	0.010(1)	0.0112(8)	0.012(1)
M1	*x*	0.37569(3)	0.3762(3)	0.3758(2)	0.3761(2)	0.3762(3)
	y	0.65408(7)	0.6560(4)	0.6558(3)	0.6564(3)	0.6566(6)
	z	0.8681(1)	0.8650(9)	0.8619(8)	0.8616(7)	0.8576(11)
	U_{11}	0.0074(3)	0.008(3)	0.006(2)	0.004(2)	0.008(3)
	U_{22}	0.0067(3)	0.005(1)	0.009(1)	0.006(1)	0.006(2)
	U_{33}	0.0061(3)	0.009(3)	0.007(4)	0.013(2)	0.006(4)
	U_{12}	−0.0000(2)	0.002(2)	−0.001(1)	−0.004(2)	−0.001(2)
	U_{13}	−0.0007(2)	−0.001(2)	−0.00(1)	−0.000(1)	−0.003(2)
	U_{23}	0.0004(2)	−0.000(3)	0.004(2)	0.002(2)	0.005(3)
	U_{eq}/U_{iso}	0.0067(2)	0.007(1)	0.008(1)	0.0079(7)	0.007(1)
TA	*x*	0.27146(3)	0.2710(2)	0.2710(1)	0.2711(2)	0.2705(2)
	y	0.34153(5)	0.3411(4)	0.3427(2)	0.3423(2)	0.3437(4)
	z	0.04929(9)	0.0448(8)	0.0428(7)	0.0408(6)	0.0376(8)
	U_{eq}/U_{iso}	0.0055(2)	0.0064(9)	0.0057(5)	0.0054(6)	0.0051(9)
O1A	*x*	0.18349(7)	0.1830(5)	0.1824(3)	0.1826(4)	0.1821(6)
	y	0.3397(1)	0.3406(8)	0.3398(6)	0.3409(6)	0.3407(12)
	z	0.0365(2)	0.0340(18)	0.0278(17)	0.0298(14)	0.0237(22)
	U_{eq}/U_{iso}	0.0067(3)	0.005(2)	0.007(1)	0.009(1)	0.007(2)
O2A	*x*/*a*	0.31076(7)	0.3102(5)	0.3099(3)	0.3097(4)	0.3092(6)
	y/*b*	0.5022(1)	0.5041(8)	0.5042(6)	0.5068(6)	0.5057(11)
	z/*c*	0.0436(2)	0.0368(19)	0.0344(18)	0.0371(13)	0.0355(21)
	U_{eq}/U_{iso}	0.0082(3)	0.007(2)	0.009(1)	0.008(1)	0.003(2)
O3A	*x*/*a*	0.30291(7)	0.3035(5)	0.3030(3)	0.3036(4)	0.3035(6)
	y/b	0.2246(2)	0.2255(8)	0.2255(6)	0.2258(6)	0.2218(10)
	z/*c*	0.8286(3)	0.8270(21)	0.8201(17)	0.8208(16)	0.8147(26)
	U_{eq}/U_{iso}	0.0088(3)	0.005(2)	0.007(1)	0.006(1)	0.008(2)
TB	*x*/*a*	0.47419(3)	0.4740(2)	0.4736(1)	0.4739(2)	0.4736(2)
	y/*b*	0.33778(5)	0.3376(4)	0.3382(3)	0.3388(3)	0.3382(5)
	z/*c*	0.7968(1)	0.7999(9)	0.8019(7)	0.8008(6)	0.8042(9)
	U_{eq}/U_{iso}	0.0055(2)	0.0064(8)	0.0070(6)	0.0061(6)	0.0064(9)
O1B	*x*/*a*	0.56276(7)	0.5619(5)	0.5625(3)	0.5618(4)	0.5628(5)
	y/*b*	0.3400(1)	0.3396(9)	0.3396(6)	0.3396(6)	0.3395(11)
	z/*c*	0.7987(2)	0.8023(21)	0.8059(19)	0.8011(14)	0.8134(26)
	U_{eq}/U_{iso}	0.0069(3)	0.010(2)	0.010(1)	0.007(1)	0.010(2)
O2B	*x*/*a*	0.43337(7)	0.4337(5)	0.4337(3)	0.4327(3)	0.4332(6)
	y/*b*	0.4842(1)	0.4864(9)	0.4846(6)	0.4856(6)	0.4847(10)
	z/*c*	0.6921(3)	0.6852(20)	0.6886(19)	0.6908(14)	0.6861(25)
	U_{eq}/U_{iso}	0.0100(3)	0.009(2)	0.006(1)	0.008(1)	0.006(2)
O3B	*x*/*a*	0.44767(7)	0.4472(5)	0.4467(4)	0.4459(4)	0.4458(6)
	y/*b*	0.1986(2)	0.1970(8)	0.1945(6)	0.1942(5)	0.1917(11)
	z/*c*	0.5991(2)	0.6067(22)	0.6052(17)	0.6057(15)	0.6085(26)
	U_{eq}/U_{iso}	0.0086(3)	0.009(2)	0.010(1)	0.006(1)	0.013(3)

Notes: The data at 1.76 and 3.94 GPa were measured during decompression, that one at 0 GPa is for the crystal in air. For the HP-refinements the isotropic thermal parameters, U_{iso}, are reported, whereas for the room condition refinements U_{eq} are shown.

TABLE 4. Bond lengths (Å) and polyhedral data

Pressure	0.0001 GPa	1.76 GPa	3.36 GPa	3.94 GPa	6.25 GPa
M2-O1A	2.104(1)	2.094(9)	2.091(7)	2.083(7)	2.075(11)
M2-O1B	2.074(1)	2.089(10)	2.074(7)	2.064(7)	2.067(12)
M2-O2A	2.054(1)	2.068(10)	2.053(9)	2.046(7)	2.045(12)
M2-O2B	1.998(1)	1.972(11)	1.994(9)	1.992(7)	1.966(13)
M2-O3A	2.296(1)	2.268(9)	2.267(6)	2.262(6)	2.219(10)
M2-O3B	2.481(1)	2.415(11)	2.369(8)	2.357(7)	2.298(12)
<M2-O>	2.17(18)	2.15(16)	2.14(14)	2.13(14)	2.11(12)
V (Å³)	12.670(16)	12.40(11)	12.219(84)	12.118(75)	11.69(12)
OQE	1.054	1.051	1.051	1.050	1.051
M1-O1A	2.147(1)	2.130(9)	2.103(7)	2.112(6)	2.089(11)
M1-O1A	2.032(1)	2.018(10)	2.011(8)	2.003(8)	1.996(12)
M1-O1B	2.169(1)	2.146(10)	2.139(7)	2.125(6)	2.115(11)
M1-O1B	2.063(1)	2.052(12)	2.037(9)	2.062(8)	2.002(13)
M1-O2A	2.008(1)	2.000(10)	1.990(8)	1.988(7)	1.995(11)
M1-O2B	2.047(1)	2.042(10)	2.032(7)	2.008(7)	2.008(11)
<M1-O>	2.078(65)	2.065(60)	2.052(57)	2.049(59)	2.034(53)
V (Å³)	11.820(16)	11.623(98)	11.404(76)	11.360(70)	11.10(11)
OQE	1.008	1.007	1.008	1.007	1.008
TA-O1A	1.610(1)	1.602(9)	1.604(6)	1.605(8)	1.594(11)
TA-O2A	1.589(1)	1.597(8)	1.580(6)	1.597(6)	1.567(10)
TA-O3A	1.665(1)	1.676(11)	1.647(8)	1.659(8)	1.659(12)
TA-O3A	1.645(1)	1.625(10)	1.640(8)	1.627(8)	1.631(13)
<TA-O>	1.627(34)	1.625(36)	1.618(32)	1.622(28)	1.613(40)
V (Å³)	2.181(5)	2.175(30)	2.145(23)	2.162(22)	2.115(35)
TQE	1.009	1.009	1.009	1.009	1.013
TAV	37.713	35.370	35.896	36.925	48.442
Basal tilt (°)	3.835	3.063	2.972	2.963	2.439
O3A-O3A-O3A (°)	160.40(11)	161.05(63)	161.03(45)	161.07(45)	158.23(78)
TB-O1B	1.617(1)	1.600(11)	1.608(6)	1.592(7)	1.609(11)
TB-O2B	1.588(1)	1.608(9)	1.582(7)	1.585(6)	1.581(10)
TB-O3B	1.673(1)	1.682(11)	1.684(7)	1.687(7)	1.647(14)
TB-O3B	1.672(1)	1.658(10)	1.654(9)	1.666(8)	1.688(12)
<TB-O>	1.637(42)	1.637(39)	1.632(46)	1.632(52)	1.631(46)
V (Å³)	2.237(5)	2.237(32)	2.216(24)	2.218(22)	2.210(36)
TQE	1.005	1.005	1.005	1.005	1.006
TAV	20.495	18.784	19.308	20.279	22.464
Basal tilt (°)	6.620	6.128	5.924	6.166	5.939
O3B-O3B-O3B (°)	141.49(9)	140.33(57)	138.51(33)	138.43(37)	136.59(59)

Notes: Polyhedral volumes and their standard deviations, as well as the average bond distances have been calculated using IVTON program (Balic-Zunic and Vickovic 1996). OQE and TQE are the octahedral and tetrahedral quadratic elongation, respectively (Robinson et al. 1971). TAV is the tetrahedral angle variance (Rossi et al. 1983). The basal tilt is defined as the angle between the basal plane of the tetrahedron (constituted by the O3-O2-O3 O atoms) and the plane (100).

(Angel 2000), indicate that the evolution of the unit-cell lattice parameters also is well described by a BM3 EoS, which has, therefore, been used. The resulting EoS parameters are: a_0 = 18.2719(6) Å, K_{a0} = 150.4(3.3) GPa, K'_a = 7.3(9), b_0 = 8.8323(2) Å, K_{b0} = 88.2(1.1) GPa, K'_b = 4.7(3), c_0 = 5.1942(4) Å, K_{c0} = 108.09(2.4) GPa, K'_c = 8.2(8). The linear axial compressibilities [$\beta_d = -1/d_0(\partial d/\partial P)_{T,X}$, with $d = a$, b, and c] are β_a = 0.0018(1) GPa^{-1}, β_b = 0.0030(1) GPa^{-1} and β_c = 0.0023(1) GPa^{-1}, with a compressibility scheme $\beta_b >> \beta_c >> \beta_a$.

Structural behavior

The structure of orthopyroxenes consists of alternating layers of silicate tetrahedra and $M^{2+}O_6$ octahedra parallel to the (100) plane (see, for example, Cameron and Papike 1981). The tetrahedra form infinite chains (A- and B-chains) parallel to the **c** axis. The A-chain is more extended and tetrahedra in the chain are characterized by smaller volumes. Of the two octahedral sites, the M2 site is larger and more distorted than M1. Large cations, like Ca, can only occupy the M2 site, whereas smaller cations (mainly Fe^{2+} and Mg) reside in both M2 and M1 sites. The sample studied in this work contains 7% of Ca in the M2 sites, with Mg occupying both the M2 (93%) and M1 (100%) sites. From the refinement of the intensity data collected with the crystal in air we obtain atomic coordinates that are not significantly different (±1σ) than those reported by Nestola and Tribaudino (2003).

Structural refinements at high-pressure confirm that the M2 octahedron is the most compressible polyhedron in the structure (Hugh-Jones and Angel 1994; Hugh-Jones et al. 1997). The M2 volume decreases by about 7.7% up to 6.25 GPa (Table 4, Fig. 3a) with a linear compressibility β_{VM2} = 0.0123(1) GPa^{-1}. The average <M2-O> bond distances undergo a shortening of about 2.6%, as a result of a relatively small shortening of four of the six M2-O distances (from –0.3% down to –1.6%), and a very strong compression of the longest M2-O3A and the M2-O3B

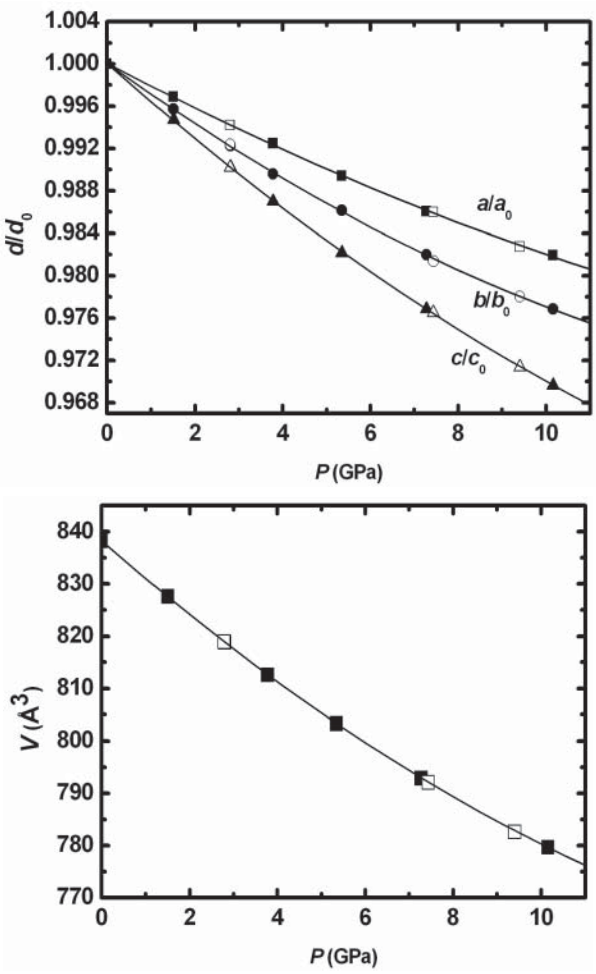

FIGURE 1. Evolution of the unit-cell parameters (**a**) and volume (**b**) as a function of pressure for Ca-bearing orthoenstatite. The open symbols refer to the measurements performed during decompression. Uncertainties are smaller than the symbols used.

bond distances (–3.4% and –7.4%, respectively). The M1 octahedron, which is smaller and more regular than M2 (Table 4), shows a smaller volume variation with pressure (–6.1%; Table 4 and Fig. 3a) with a linear compressibility β_{VM1} = 0.0097(1) GPa^{-1}. The average <M1-O> bond distances show a variation of about –2.1% with all six M1-O bond distances decreasing between 0.6% (M1-O2A) and 3% (M1-O1B).

The pressure dependence of the volumes of the SiO_4 tetrahedra TA and TB of the A-chain and B-chain, respectively, is shown in Figure 3b. The volumes of TA and TB decrease by about 3% and 1.2%, respectively, vary linearly with pressure and exhibit no discontinuities in the pressure range investigated. The chain kinking expressed in terms of the O3-O3-O3 angle decreases by 1.4% for the A-chain and by 3.5% for the B-chain (Table 4). The basal tilt, defined as the angle between the basal plane of the tetrahedron (defined by O3-O2-O3) and (100), decreases linearly as a function of pressure, with a variation by about 1.4° for the A-chain and about 0.7° for the B-chain (Table 4).

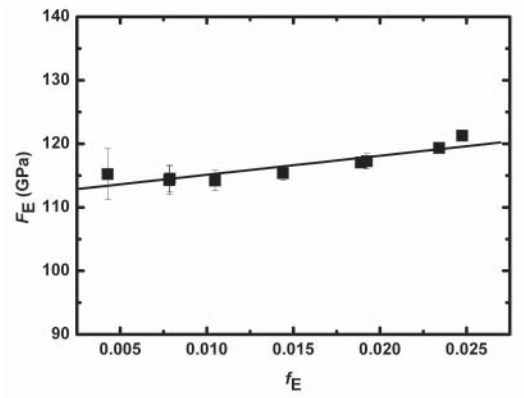

FIGURE 2. F_E-f_E plot. From the linear fit one obtains $F_E = K_{T0}$ = 112(1) GPa for $f_E = 0$ and K' = (slope/3K_{T0}) × 2 + 4 = 6(1). The value of K_{T0} and K' so calculated are in good agreement with those obtained by fitting the *P*-*V* data with a BM3 EoS.

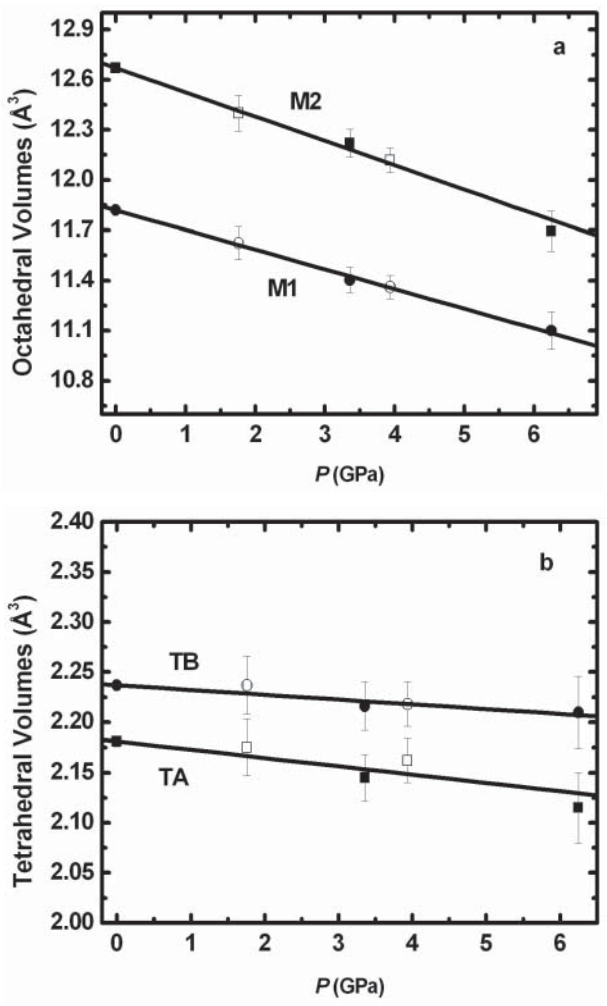

FIGURE 3. Evolution of the octahedral (**a**) and tetrahedral (**b**) volumes as a function of pressure for Ca-bearing orthoenstatite of this study. The values at 0.0001 GPa are from the structure refinement with the crystal in air. The open symbols refer to the measurements during decompression.

DISCUSSION

Effect of Ca on the elastic behavior of pure orthoenstatite

A comparison between the EoS parameters obtained for pure orthoenstatite (Angel and Jackson 2002) and those obtained in this study reveals that the substitution of 7% of Ca for Mg gives rise to a slight increase of the K_{T0} value (about 3.6%) and to a decrease of the K' value (about 22%). This variation of the elastic behavior of orthoenstatite due to Ca substitution is very similar to that observed for a natural orthopyroxene, which contains both Ca and Al and is stiffer than our sample (Hugh-Jones et al. 1997). We, therefore, exclude the possibility that such effects might be due to clinopyroxene lamellae, which are present at practically negligible levels (estimated to be less than 0.1% by volume based on TEM observations).

Ca substitution in monoclinic pyroxenes has the opposite effect on bulk modulus and its pressure derivative. For $P2_1/c$ clinopyroxenes along the join diopside-clinoenstatite (Angel and Hugh-Jones 1994; Nestola et al. 2004) it has been found that the substitution of 15% Ca into the pure clinoenstatite structure decreases the value of K_{T0} from 111.1(3.3) to 102(2) GPa and increases the value of K' from 6.6(1.1) to 8(1).

Structural evolution of orthopyroxenes with pressure

To understand the effect of Ca substitution on the deformation mechanism of the orthopyroxene structure, we can compare our results with those obtained for a synthetic pure orthoenstatite (Hugh-Jones and Angel 1994), for a synthetic sample with composition $Mg_{0.6}Fe_{0.4}SiO_3$ (En60) (Hugh-Jones et al. 1997) and for a natural orthopyroxene with composition $(Mg_{0.83}Fe_{0.12}Ca_{0.006}Al_{0.04})(Si_{0.97}Al_{0.03})O_3$ (Oen-nat; Hugh-Jones et al. 1997). For all samples, the M2 polyhedron undergoes the largest deformation. This is mainly due to the very large variation shown by the M2-O3A and M2-O3B bond distances. The M2-O3B bond distance decreases at a greater rate than M2-O3A for all the samples except Oen-nat (Fig. 4). The stiffening of the M2-O3B bond in the natural sample may be a consequence of its smaller tetrahedral B-chain kinking with respect to the synthetic pyroxenes, which gives rise to a shorter M2-O3B distance. It appears therefore that the stiffening of the M2-O3B bond in the natural orthopyroxene is not directly related to the Ca substitution into the M2 site, but more likely to some secondary effect such as the presence of Al at the M1 site.

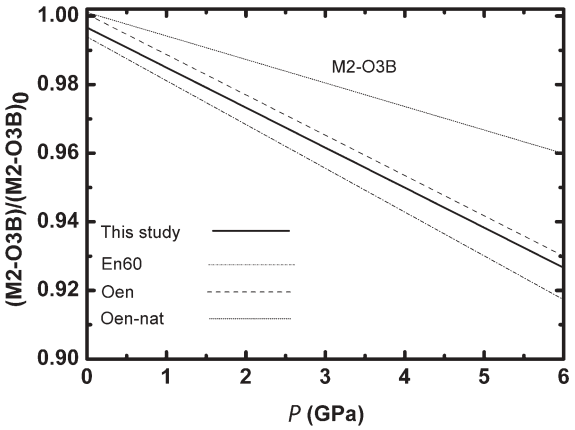

FIGURE 4. Evolution of the M2-O3B bond distances as a function of pressure. For clarity only the trend-lines of the (M2-O3B)/(M2-O3B)$_0$ ratios vs. P are plotted. Data for En60 and Oen-nat are from Hugh-Jones et al. (1997); data for Oen are from Angel and Hugh-Jones (1994).

The other major difference between the high-pressure structural behavior of the Oen-nat and $(Mg,Fe)SiO_3$ orthopyroxenes is related to the compressibility of the TA and TB tetrahedra (Hugh-Jones et al. 1997). Whereas the tetrahedra of the Oen-nat sample are relatively incompressible up to 6 GPa, the tetrahedra of pure orthoenstatite (Hugh-Jones and Angel 1994) and En60 show a change in their compressibility behavior at about 3–4 GPa. Our Ca-bearing sample shows an intermediate behavior: both TA and TB are more compressible, but do not show any discontinuity in the evolution of their volumes with pressure (Fig. 3b). Thus, although the Ca substitution clearly affects the tetrahedral behavior with respect to that observed for synthetic $(Mg,Fe)SiO_3$ and natural orthopyroxene, it cannot be the only factor because the presence of other cations (e.g., Al in natural orthopyroxene) can contribute to polyhedral compressibility.

High-pressure phase transition in orthopyroxenes

High-pressure Raman spectroscopic studies have reported the occurrence of a phase transformation in orthoenstatite above 10 GPa (Chopelas 1999; Lin 2003), which appears to be first order and reversible with a slight hysteresis. Chopelas (1999) suggests that the new phase is the monoclinic high-pressure $C2/c$ phase of clinoenstatite; however, it is well known that $C2/c$ clinoenstatite reverts to $P2_1/c$ clinoenstatite rather than orthoenstatite with decreasing pressure. For this reason, Lin (2003) suggests that the high-pressure phase is a metastable intermediate polymorph between orthoenstatite and the high-pressure clinoenstatite. Kung et al. (2004) observe an anomalous behavior of the elastic wave velocities V_P and V_S for orthoenstatite above 9 GPa, which appears to be associated with a reversible phase transformation. On the basis of their X-ray powder-diffraction patterns, they suggest that this high-pressure polymorph is a metastable phase related to the kinetics of the phase transition from orthoenstatite to HP-clinoenstatite at room temperature. However, this phase is different from the *Cmca* phase suggested by Jackson et al. (2004) from their high-temperature experiments of orthoenstatite at room pressure. The *Pbca* → HP-$C2/c$ phase transition has indeed been observed for orthoferrosilite by in-situ single-crystal X-ray diffraction above 4.2 GPa (Hugh-Jones et al. 1996), and it appears to be highly time-dependent. No discontinuity in the unit-cell parameter evolution was observed for our sample up to 10.16 GPa, suggesting that no phase transition occurs in the pressure range investigated. The crystal, however, was kept at pressure above 9.4 GPa only for a total of 7 days, therefore it is not possible to determine if the Ca substitution increases the stability field of pure orthoenstatite, or if the time-scale of our experiment was too short to observe any anomaly in our crystal.

ACKNOWLEDGMENTS

This project was supported by the Alexander von Humboldt Foundation to Fabrizio Nestola and by the S. Kovalevskaja Award to Tiziana Boffa Ballaran. The manuscript benefited from constructive reviews by A. Pawley, J. Jackson, H.P. Liermann, and by an anonymous referee.

REFERENCES CITED

Allan, D.R., Miletich, R. and Angel, R.J. (1996) A diamond-anvil cell for single-crystal X-ray diffraction studies to pressures in excess of 10 GPa. Review Scientific Instruments, 67, 840–842.

Angel, R.J. (2000) Equations of State. In R.M. Hazen and R.T. Downs, Eds., High-temperature and high-pressure crystal chemistry, 41, p. 35–39. Reviews in Mineralogy and Geochemistry, Mineralogical Society of America, Chantilly, Virginia.

——— (2001) EOS-FIT V5.2 program. Crystallography Laboratory, Department of Geological Sciences, Virginia Tech, Blacksburg, Virginia.

——— (2003) Automated profile analysis for single-crystal diffraction data. Journal of Applied Crystallography, 36, 295–300.

——— (2004) Absorption corrections for diamond-anvil cells implemented in the software package Absorb 6.0. Journal of Applied Crystallography, 37, 486–492.

Angel, R.J. and Hugh-Jones, D.A. (1994) Equation of state and thermodynamic properties of enstatite pyroxenes. Journal of Geophysical Research, 99, 19777–19783.

Angel, R.J. and Jackson, M.J. (2002) Elasticity and equation of state of orthoenstatite, $MgSiO_3$. American Mineralogist, 87, 558–561.

Angel, R.J., Downs, R.T., and Finger, L.W. (2000) High-Temperature-High-Pressure diffractometry. In R.M. Hazen and R.T. Downs, Eds., High-temperature and high-pressure crystal chemistry, 41, p. 559–596. Reviews in Mineralogy and Geochemistry, Mineralogical Society of America, Chantilly, Virginia.

Balic-Zunic, T. and Vickovic, I. (1996) IVTON program for the calculation of geometrical aspects of crystal structures and some chemical applications. Journal of Applied Crystallography, 29, 305–306.

Bass, J.D. and Weidner, D.J. (1984) Elasticity of single-crystal orthoferrosilite. Journal of Geophysical Research, 89, 4359–4371.

Birch, F. (1947) Finite elastic strain of cubic crystals. Physical Review, 71, 809–824.

Cameron, M. and Papike, J.J. (1981) Structural and chemical variations in pyroxenes. American Mineralogist, 66, 1–50.

Chai, M., Brown, M., and Slutsky, L.J. (1997) The elastic constants of an aluminous orthopyroxene to 12.5 GPa. Journal of Geophysical Research, 102, 14779–14785.

Chatillon-Colinet, C., Newton, R.C., Perkins, D., III, and Kleppa, O.J. (1983) Thermochemistry of $(Fe^{2+},Mg)SiO_3$ orthopyroxene. Geochimica et Cosmochimica Acta, 47, 1597–1603.

Chopelas, A. (1999) Estimates of mantle relevant Clapeyron slopes in the $MgSiO_3$ system from high-pressure spectroscopic data. American Mineralogist, 84, 233–244.

——— (2000) Thermal expansivity of mantle relevant magnesium silicates derived from vibrational spectroscopy at high-pressure. American Mineralogist, 85, 270–278.

Chopelas, A. and Boehler, R. (1992) High-pressure research: application to Earth and Planetary Sciences. In Y. Syono and M.H. Manghnani, Eds., 101 p. Terra Scientific, Tokyo.

Domeneghetti, M.C. and Steffen, G. (1992) M1, M2 site populations and distortion parameters in synthetic Mg-Fe orthopyroxenes from Mössbauer spectra and X-ray structure refinements. Physics and Chemistry of Minerals, 19, 298–306.

Domeneghetti, M.C., Molin, G.M., and Tazzoli, V. (1995a) A crystal-chemical model for *Pbca* orthopyroxenes. American Mineralogist, 80, 253–267.

Domeneghetti, M.C., Molin, G.M., Stimpfl, M., and Tribaudino, M. (1995b) Orthopyroxene from Serra de Mage' meteorite: structure refinement and estimation of *C*2/*c* pyroxene contributions to apparent *Pbca* diffraction violations. American Mineralogist, 80, 923–929.

Domeneghetti, M.C., Molin, G.M., Triscari, M., and Zema, M. (2000) Orthopyroxenes as a geospeedometer: thermal history of Kapoeta, Old Homestead 001 and Hughes 004 howardites. Meteoritics and Planetary Science, 35, 347–354.

Duffy, T.S. and Vaughan, M.T. (1988) Elasticity of enstatite and its relationship to crystal structure. Journal of Geophysical Research, 93, 383–391.

Flesch, L.M., Li, B., and Liebermann, R.C. (1998) Sound velocities of polycrystalline $MgSiO_3$-orthopyroxene to 10 GPa at room temperature. American Mineralogist, 83, 444–450.

Frisillo, A.L. and Barsch, G.R. (1972) Measurement of single-crystal elastic constants of bronzite as a function of pressure and temperature. Journal of Geophysical Research, 77, 6360–6384.

Ganguly, J., Yang, H.X., and Ghose, S. (1994) Thermal history of mesosideritesóQuantitative constraints from compositional zoning and Fe-Mg ordering in orthopyroxenes. Geochimica and Cosmochimica Acta, 58, 2711–2723.

Goodrich, C.A. (2003) Petrogenesis of olivine-phyric shergottites Sayh Al Uhaymir 005 and Elephant Moraine A79001 lithology A. Geochimica et Cosmochimica Acta, 67, 3735–3772.

Goodrich, C.A., Fioretti, A.M., Tribaudino, M., and Molin, G.M. (2001) Primary trapped melt inclusions in olivine in the olivine-augite-orthopyroxene ureilites Hughes 009. Geochimica and Cosmochimica Acta, 65, 621–652.

Hawthorne, F.C. and Ito, J. (1977) Synthesis and crystal structure refinement of transition-metal orthopyroxenes. I: orthoenstatite and (Mg, Mn, Co) orthopyroxene. Canadian Mineralogist, 15, 321–338.

Hugh-Jones, D.A. (1997) Thermal expansion of $MgSiO_3$ and $FeSiO_3$ ortho- and clinopyroxenes. American Mineralogist, 82, 689–696.

Hugh-Jones, D.A. and Angel, R.J. (1994) A compressional study of $MgSiO_3$ orthoenstatite up to 8.5 GPa. American Mineralogist, 79, 405–410.

Hugh-Jones, D.A., Sharp, T., Angel, R.J., and Woodland, A. (1996) The transition of orthoferrosilite to high-pressure C2/c clinoferrosilite at ambient temperature. European Journal of Mineralogy, 8, 1337–1345.

Hugh-Jones, D.A., Chopelas, A., and Angel, R.J. (1997) Tetrahedral compression in $(Mg,Fe)SiO_3$ orthopyroxenes. Physics and Chemistry of Minerals, 24, 301–310.

Ito, H., Mizutani, H., Ichinose, K., and Akimoto, A. (1977) Ultrasonic wave velocity measurements in solids under high pressure using solid media. In M. Manghanni and S. Akimoto, Eds., High-pressure Research: Applications in Geophysics, p. 620–630. Academic Press, New York.

Jackson, J.M., Sinogeikin, S.V., and Bass, J.D. (1999) Elasticity of $MgSiO_3$ orthoenstatite. American Mineralogist, 84, 677–680.

Jackson, J.M., Palko, J., Sinogeikin, S.V., Bass, J.D., Andrault, D., and Zha, C. (2001) High-temperature single-crystal elasticity and thermal expansion of orthoenstatite. Eos (Fall Meet. Suppl.), Abstract T31C-0853.

Jackson, J.M., Sinogeikin, S.V., Carpenter, M.A., and Bass, J.D. (2004) Novel phase transition in orthoenstatite. American Mineralogist, 89, 239–245.

Kung, J., Li, B.S., Uchida, T., Wang, Y.B., Neuville, D., and Liebermann, R.C. (2004) In situ measurements of sound velocities and densities across the orthopyroxeneóhigh-pressure clinopyroxene transition in $MgSiO_3$ at high-pressure. Physics of the Earth and Planetary Interiors, 147, 27–44.

Lin, C.C. (2003) Pressure-induced metastable phase transition in orthoenstatite ($MgSiO_3$) at room temperature: a Raman spectroscopic study. Journal of Solid State Chemistry, 174, 403–411.

Mao, H.K., Xu, J., and Bell, P.M. (1986) Calibration of the ruby pressure gauge to 800 kbar under quasi-hydrostatic conditions. Journal of Geophysical Research, 91, 4673–4676.

Molin, G.M., Domeneghetti, M.C., Salviulo, G., Stimpfl, M., and Tribaudino, M. (1994) Antartic FRO90011 lodranite: cooling history from pyroxene crystal chemistry and microstructure. Earth and Planetary Science Letters, 128, 479–487.

Morimoto, N. and Koto, K. (1969) The crystal structure of orthoenstatite. Zeitschrift für Kristallographie, 129, 65–83.

Nestola, F. and Tribaudino, M. (2003) The structure of Pbca orthopyroxenes along the join diopside-enstatite ($CaMgSi_2O_6$-$Mg_2Si_2O_6$). European Journal of Mineralogy, 15, 365–371.

Nestola, F., Tribaudino, M., and Boffa Ballaran, T. (2004) High-pressure behavior, transformation and crystal structure of synthetic iron-free pigeonite. American Mineralogist, 89, 189–196.

Ohashi, Y. (1984) Polysynthetically-twinned structures of enstatite and wollastonite. Physics and Chemistry of Minerals, 10, 217–229.

Ralph, R.L. and Finger, L.W. (1982) A computer program for refinement of crystal orientation matrix and lattice constraints from diffractometer data with lattice symmetry constraints. Journal of Applied Crystallography, 15, 537–539.

Ralph, R.L. and Ghose, S. (1980) Enstatite, $Mg_2Si_2O_6$: compressibility and crystal structure at 21 kbar (abs). Eos, 61, 409.

Robinson, K., Gibbs, G.V., and Ribbe, P.H. (1971) Quadratic elongation; a quantitative measure of distortion in coordination polyhedra. Science, 172, 567–570.

Rossi, G., Smith, D.C., Ungaretti, L., and Domeneghetti, M.C. (1983) Crystal-chemistry and cation ordering in the system diopside-jadeite: a detailed study by crystal structure refinement. Contributions to Mineralogy and Petrology, 83, 247–258.

Sheldrick, G.M. (1997) Programs for Crystal Structure Analysis (Release 97-2). Institüt für Anorganische Chemie der Universität, Tammanstrasse 4, D-3400 Göttingen, Germany, 1998.

Skogby, H., Annersten, H., Domeneghetti, M.C., Molin, G.M., and Tazzoli, V. (1992) Iron distribution in orthopyroxene: a comparison of Mössbauer spectra and X-ray refinement results. European Journal of Mineralogy, 4, 441–452.

Stimpfl, M., Ganguly, J., and Molin, G.M. (1999) Fe^{2+}-Mg order-disorder in orthopyroxene: equilibrium fractionation between octahedral sites and thermodynamic analysis. Contribution to Mineralogy and Petrology, 136, 297–309.

Tribaudino, M. and Nestola, F. (2002) Average and local structure in $P2_1/c$ clinopyroxenes along the join diopside-enstatite ($CaMgSi_2O_6$). European Journal of Mineralogy, 14, 549–555.

Webb, S.L. and Jackson, I. (1993) the pressure dependence of the elastic moduli of single-crystal orthopyroxene $(Mg_{0.8}Fe_{0.2})SiO_3$. European Journal of Mineralogy, 5, 1111–1119.

Weidner, D.J., Wang, H., and Ito, J. (1978) Elasticity of orthoenstatite. Physics of the Earth and Planetary Interiors, 17, 7–13.

Wilson, A.J.C., Ed. (1995) International Tables for Crystallography, vol. C. Kluwer Academic Publishers, Dordrecht, The Netherlands.

Woodland, A.B. (1998) The orthorhombic to high-*P* monoclinic phase transition

in Mg-Fe pyroxenes. Can it produce a seismic discontinuity? Geophysical Research Letters, 25, 1241–1244.
Yang, H. and Ghose, S. (1994) In situ Fe-Mg order-disorder studies and thermodynamic properties of orthopyroxene $(Fe,Mg)_2Si_2O_6$. American Mineralogist, 79, 633–643.
——— (1995a) High-temperature single-crystal X-ray diffraction studies of the ortho-proto phase transition in enstatite, $Mg_2Si_2O_6$ at 1360 K. Physics and Chemistry of Minerals, 22, 300–310.
——— (1995b) A transitional structural state and anomalous Fe-Mg order-disorder in Mg-rich orthopyroxene, $(Mg_{0.75}Fe_{0.25})Si_2O_6$. American Mineralogist, 80, 9–20.
Zema, M., Domeneghetti, M.C., and Molin, G.M. (1996) Thermal history of Acapulco and ALHA81261 acapulcoites constrained by Fe^{2+}-Mg ordering in orthopyroxene. Earth and Planetary Science Letters, 144, 359–367.
Zema, M., Domeneghetti, M.C., Molin, G.M., and Tazzoli, V. (1997) Cooling rates of diogenites: a study of Fe^{2+}-Mg ordering in orthopyroxene by single-crystal X-ray diffraction. Meteoritics and Planetary Science Letters, 32, 855–862.
Zema, M., Domeneghetti, M.C., and Tazzoli, V. (1999) Order-disorder kinetics in orthopyroxene with exsolution products. American Mineralogist, 84, 1895–1901.
Zema, M., Tarantino, S.C., Domeneghetti, M.C., and Tazzoli, V. (2003) Ca in orthopyroxene: structural variations and kinetics of the disordering process. European Journal of Mineralogy, 15, 373–380.
Zhao, Y., Schiferl, D., and Shankland, T.J. (1995) A high *P-T* single-crystal X-ray diffraction study of thermoelasticity of $MgSiO_3$ orthoenstatite. Physics and Chemistry of Minerals, 22, 393–398.

MANUSCRIPT RECEIVED MAY 12, 2005
MANUSCRIPT ACCEPTED DECEMBER 25, 2005
MANUSCRIPT HANDLED BY ALISON PAWLEY